

**Redox Sensitive Protein Droplets from Recombinant Oleosin**

Journal:	<i>Soft Matter</i>
Manuscript ID	SM-ART-05-2018-001047.R1
Article Type:	Paper
Date Submitted by the Author:	12-Jul-2018
Complete List of Authors:	Reed, Ellen; University of Pennsylvania, Chemical Engineering Hammer, Daniel; University of Pennsylvania, Department of Bioengineering



Redox Sensitive Protein Droplets from Recombinant Oleosin

Ellen H. Reed^a and Daniel A. Hammer^{*a,b}

Received 00th January 20xx,
Accepted 00th January 20xx

DOI: 10.1039/x0xx00000x

www.rsc.org/

Protein engineering enables the creation of materials with designer functionality and tailored responsiveness. Here, we design a protein with two control motifs for its phase separation into micron sized liquid droplets – one driven by a hydrophobic domain and the other by oxidation of a disulfide bond. Our work is based on the plant surfactant protein, oleosin, which has a hydrophobic domain but no cysteines. Oleosin phase separates to form liquid droplets below a critical temperature akin to many naturally occurring membrane-less organelles. Sequence mutations are made to introduce a cysteine residue into oleosin. The addition of a cysteine causes phase separation at a lower concentration and increases the phase transition temperature. Adding a reducing agent to phase-separated, cysteine-containing oleosin rapidly dissolves the droplets. The transition temperature can be tuned by varying the location of the cysteine or by blending the parent cysteine-less molecule with the cysteine containing mutant. This provides a novel way to control protein droplet formation and dissolution. We envision this work having applications as a system for the release of a protein or drug with engineered sensitivity to reducing conditions and as a mimic of membrane-less organelles in synthetic protocells.

Introduction

Liquid-liquid phase separation of proteins has gained increased interest recently due to its regulatory role in cells.^{1,2} There are many natural proteins that, under appropriate conditions, condense to form liquid droplets, known as membrane-less organelles. These droplets, which concentrate proteins and other bioactive agents, can regulate various processes in cells through the localized condensation of high concentrations of relevant molecules.³ Examples include stress-granules, P-granules, Cajal bodies, and nucleoli.⁴ Proteins that undergo this type of phase transition can be exploited to create responsive biomolecular materials.⁵⁻⁸

Work has been done to identify features common to proteins that undergo a liquid-liquid phase transition.⁹⁻¹¹ Proteins that condense into droplets are often zwitterionic and enriched in charged residues. Complex coacervation resulting from charged residues acts as a driving force for droplet condensation.^{12,13} Phase separating proteins also tend to be hydrophilic. Furthermore, many proteins that exhibit a liquid-liquid phase transition have low complexity, intrinsically disordered regions.^{14,15} In some proteins, the intrinsically disordered region is necessary and sufficient to drive phase separation.¹⁶ Another common driving force for liquid-liquid

phase transition of proteins is multivalent interactions.^{17,18} In the case of γ -crystallin, an eye lens protein, formation of oligomers via oxidation of a disulfide bond potentiates droplet formation.^{19,20}

We can use knowledge of features that drive phase separation to engineer a protein with controllable phase behavior. Engineered, responsive, recombinant proteins are increasingly being designed for many applications such as targeted drug delivery and artificial protocells.²¹⁻²³ Unlike polymeric materials, recombinant proteins are monodisperse and allow for precise control over the monomer (amino acid) sequence. Here, we use the tools of recombinant biotechnology to create an amphiphilic molecule that can undergo a phase transition. Furthermore, by introduction of a cysteine residue to a precise location, we can drive phase separation through an oxidative switch. This molecule adds to the palette of tunable materials that can be used for drug delivery and in artificial protocells.

In this work, we use a naturally occurring amphiphilic plant protein, oleosin, to engineer liquid protein droplets. Oleosin is an ideal candidate for engineered protein droplets due to its amenability to modifications and its similarity to other proteins that form membrane-less organelles. In nature, oleosin stabilizes oil bodies in seeds.^{24,25} It contains a central hydrophobic domain that resides in the oil phase of oil bodies and is thought to be α -helical.²⁶ The hydrophobic domain is flanked by hydrophilic domains that reside in the surrounding cytosol. Three highly conserved prolines in the hydrophobic section are hypothesized to form a proline knot and induce a 180° turn, bifurcating the protein and leading to the formation of a hairpin.²⁷ The hydrophilic domains of oleosin are

^a Department of Chemical and Biomolecular Engineering, University of Pennsylvania, Philadelphia, PA 19104, USA.

^b Department of Bioengineering, University of Pennsylvania, Philadelphia, PA 19104, USA

E-mail: hammer@seas.upenn.edu

Electronic Supplementary Information (ESI) available: See DOI: 10.1039/x0xx00000x

zwitterionic and are predicted to be disordered which are common features in proteins that form membrane-less organelles.

Oleosin has been extensively engineered to form useful materials. Artificial oil bodies stabilized by oleosins have been used for food, cosmetics, and manufacturing.^{28,29} Oleosin stabilized oil bodies have also been suggested as a drug delivery system^{30,31} Furthermore, oleosin has been used in the synthesis of biopharmaceuticals.^{32,33} Oleosin-therapeutic fusions are expressed in plants, then the oil bodies are harvested and the therapeutic molecule is recovered by cleaving it from the oleosin. By using aqueous systems rather than oil bodies, a variety of oleosin suprastructures have been made. Oleosin micelles, fibers, sheets, and vesicles were all formed by modifying the lengths of the hydrophobic and hydrophilic domains.^{34,35} Using recombinant methods, one oleosin variant has been engineered to include an integrin binding motif, RGDS,³⁶ another has been engineered to contain an affibody for binding to a cell surface receptor.³⁷

We engineered oleosin to form redox responsive droplets. The starting molecule for this study was a truncated version of oleosin, referred to as Oleo30G.³⁴ To form Oleo30G, the hydrophobic core of oleosin was shortened from 87 residues to 30, removing several threonine residues, and five glycine residues were added to increase chain flexibility. Oleo30G has been shown to form spherical micelles above a critical micelle concentration (cmc) of approximately 10 μ M driven by hydrophobic interactions. The hydrophobic portion of the protein is buried in the core of the micelle while the hydrophilic N- and C-terminal segments form the corona. However, we found that at higher concentrations, Oleo30G will assemble into protein droplets. Because neither wildtype oleosin nor Oleo30G contain any cysteine residues, we postulated that the addition of cysteines, would be a means of introducing advanced functionality, such as the formation of disulfide bonds between oleosins.

We demonstrate that the addition of a cysteine residue to Oleo30G, causes liquid-liquid phase separation to be induced at a lower concentration. Furthermore, the transition temperature for phase separation can be controlled by varying the position of the cysteine residue or by blending a cysteine containing mutant with the parent cysteine-less molecule. Oleo30G-cys droplets dissolved upon the addition of a reducing agent to break the disulfide bond. Therefore, we have made an amphiphilic protein that that can be induced to phase separate with two switches – hydrophobic interactions and disulfide bonding.

Experimental

Gene creation and protein expression

Modifications to the oleosin gene to mutate residues to a cysteine were done via polymerase chain reaction. Genes were contained in the expression vector, pBamUK, a pET derivative. A 6-histidine tag was included at the C-terminus for IMAC purification. Proteins were expressed in *e. coli*

BL21(DE3) cells (Stratagene). A 5 mL starter culture was grown up overnight at 37 °C in Luria broth (Sigma Aldrich, St. Louis, MO, USA) with 50 μ g/mL kanamycin (Amresco, Solon, OH, USA). 500 mL of terrific broth (Fisher Scientific, Hampton, NH, USA) with 50 μ g/mL kanamycin was inoculated with the starter culture and grown at 37 °C while shaking at 250 rpm until the optical density at 600 nm reached 0.4-0.7. Expression was induced with isopropyl- β -D-1-thiogalactoside (Lab Scientific, Highlands, NJ, USA) at a final concentration of 0.5 mM. The culture was then grown at 37 °C for 4 hours. Cells were harvested by centrifugation and stored at -20 °C until purification.

Protein purification

Cells were lysed with 20 mL of bacterial protein extraction reagent per 500 mL culture (Thermo Fisher Scientific, Waltham, MA, USA) with 1 μ g/mL DNase (Roche, Basel, Switzerland) and 2 mg/mL lysozyme (Thermo Fisher Scientific). The lysate was centrifuged at 15,000 RCF for 15 minutes. The protein was present in inclusion bodies in the insoluble fraction after centrifugation. The insoluble fraction was resuspended in 8 M urea (Fisher Scientific) to solubilize the inclusion bodies and the solution was centrifuged at 15,000 RCF for 15 minutes to remove cell debris. Purification was carried out on an Akta FPLC with a 1 mL Ni-NTA His-Trap column (GE Healthcare Life Sciences, New York, NY, USA). Protein was bound to the column and the column was washed with urea wash buffer (8 M urea, 500 mM NaCl, 20 mM Tris (Bio-Rad, Hercules, CA, USA), 20 mM imidazole (Thermo Fisher Scientific), 5 mM DTT (Fisher Scientific). Urea concentration was gradually decreased to zero over 30 minutes to allow for protein refolding. Protein was eluted with a high imidazole elution buffer (500 mM NaCl, 20 mM Tris, 500 mM imidazole, 5 mM DTT). Fractions containing protein were pooled and 1 mL aliquots were flash frozen in liquid nitrogen and stored at -80 °C. Protein aliquots were thawed and dialyzed into DPBS (Thermo Fisher Scientific) with 1 mM DTT. Dialysis was carried out at room temperature in 1 kDa MWCO dialysis tubing (Spectrum Labs, Rancho Dominguez, CA, USA). The dialysis buffer was changed three times at least 1 hour apart and let run over night after the last buffer exchange. After dialysis, the protein was centrifuged at 6,000 RCF for 2 minutes to remove any aggregates. Protein concentration was determined by measuring the absorbance 280 nm on a NanoDrop (Thermo Fisher Scientific).

SDS-PAGE

Protein samples were denatured with NuPAGE sample buffer, reduced with NuPAGE reducing agent (Invitrogen, Carlsbad, CA), and heated at 70 °C for 10 minutes. Samples were run on NuPAGE Novex 4-12% Bis-Tris gels (Invitrogen). Gels were run for 35 minutes at 200 V. Gels were stained with Instant Blue (Expedeon, Cambridgeshire, UK) following the manufacturer's protocol.

MALDI-TOF-MS

The molecular weights of proteins were confirmed using MALDI-TOF-MS. Spots consisting of 1 μL of protein solution and 1 μL matrix solution (10 mg/mL sinapinic acid (Sigma Aldrich) dissolved in 50:50 acetonitrile (Fisher Scientific):water with 0.1% trifluoroacetic acid (Fisher Scientific)) were applied to a MTP 384 polished steel target plate (Bruker, Billerica, MA, USA). Spectra were collected on an Ultraflextreme MALDI-TOF-MS (Bruker).

Dynamic light scattering

DLS was used to probe self-assembly of oleosin mutants at low concentrations. 75 μL of protein solution at 30 μM protein in DPBS with 1 mM DTT was added to a micro-cuvette (Brand GMBH, Wertheim, Germany). DLS was conducted on a Malvern Zetasizer Nano ZS (Westborough, MA, USA). Measurements were taken at room temperature.

Pyrene assay

The cmc of oleosin mutants was determined using the fluorescent probe, pyrene. A protein dilution series in DPBS was made with concentrations ranging from 0.001 to 100 μM . Pyrene was dissolved in ethanol and added to the protein solutions to a final concentration of 0.6 μM . The emission spectra were measured on a Fluoromax-3 spectrophotometer (Horiba Scientific, Edison, NJ, USA) using an excitation of 334 nm and measuring emission from 350 to 400 nm. The ratio of the intensities of the first and third peaks in the emission spectrum was plotted as a function of protein concentration. A sigmoidal curve was fit to the data. The cmc was determined as the inflection point of this curve.

Circular Dichroism

Circular dichroism spectra of oleosin mutants were collected on an Aviv Model 425 Circular Dichroism Spectrometer (Aviv Biomedical, Lakewood, NJ, USA). 15 μM protein samples were prepared in 10 mM Na_2HPO_4 with 140 mM NaF. NaF was used in lieu of NaCl because Cl^- ions absorb strongly below 195 nm. Spectra were collected from 260 nm to 190 nm in 1 nm increments in a 1 mm light path Quartz Suprasil cuvette (Hellma Analytics, Müllheim, Germany). Data were analyzed using CDPro.³⁸ Estimations of secondary structure fractions were made using the CONTIN, SELCON3, and CDSSTR algorithms. The average of the three estimations is reported.

UV-VIS Spectroscopy

Temperature dependent ultraviolet-visible spectroscopy was used to measure the turbidity of protein solutions. The absorbance was measured at 600 nm on a UV-vis spectrophotometer (Cary 100 Bio, Agilent, Santa Clara, CA, USA). 600 μL of protein solution at 80 μM protein in DPBS with 1 mM DTT was added to a 1 cm path length quartz cuvette (Thorlabs, Newton, NJ, USA). The sample was equilibrated at 37 $^\circ\text{C}$ then cooled to 0 $^\circ\text{C}$ at a rate of 1 $^\circ\text{C}$ per

minute. Absorbance during droplet dissolution was measured by heating from 0 $^\circ\text{C}$ to 42 $^\circ\text{C}$ at a rate of 1 $^\circ\text{C}$ per minute. The absorbance was measured every 0.5 $^\circ\text{C}$.

Microscopy

Imaging was conducted on a Leica DMI8 inverted microscope using a 63x, 1.4 NA plan-apochromatic oil-immersion objective and a 0.55 NA condenser and an sCMOS camera (Orca Flash 4.0, Hamamatsu Photonics, Hamamatsu, Japan). 100 μL of protein solution was added to chambered coverglass (No. 1.5 glass thickness, Molecular Probes, Eugene, OR, USA). The chambered coverglass was coated with pluronic F-127 to block protein adhesion. A solution of 5% F-127 pluronic was added to the chamber and let sit overnight. The chamber was rinsed with water prior to sample addition to remove excess pluronic. Images were taken at the coverglass. Phase diagrams were developed by imaging 50 μL of protein solution at the specified protein and salt concentration. Samples were chilled on ice for 10 minutes before imaging. Samples were let to settle on the coverglass before the presence of droplets was determined visually.

Results

Oleosin contains a central hydrophobic region, flanked by hydrophilic regions. To create Oleo30G, sections of the hydrophobic region of wild type (WT) oleosin were removed, leaving 30 residues in the hydrophobic core, and 5 glycines were introduced. A prediction of disorder for Oleo30G was made using the PONDR VL3-BA algorithm³⁹ and hydrophobicity was calculated using the Kyte-Doolittle scale (Figure 1a).⁴⁰ Based on PONDR, it is predicted that the hydrophilic domains of Oleo30G are disordered. These domains contain both negatively and positively charged residues. 19.4% of the residues in Oleo30G are charged with 8.6% positively charged and 10.8% negatively charged. Disordered regions, charged residues, and hydrophilicity are common among proteins that phase separate to form liquid droplets,¹²⁻¹⁶ therefore, oleosin is an ideal starting point to engineer protein droplets.

A single cysteine residue was incorporated at different locations in the N-terminal, hydrophilic region of Oleo30G, a molecule previously devoid of cysteines, to create Oleo30G-cys (Figure 1b, Table S1). The notation for the Oleo30G-cys mutants is Oleo30G_XYC where X is the residue that was mutated to a cysteine, and Y is the position of that residue. The mutations considered were: Oleo30G_S2C, Oleo30G_T3C, Oleo30G_T4C, Oleo30G_T5C, Oleo30G_T12C, Oleo30G_T24C, and Oleo30G_S39C. Residues most similar to the reduced form of cysteine, serine and threonine, were mutated. Genes were inserted into the expression vector pBamUK, which adds a 6-histidine tag on the C-terminus for immobilized metal affinity chromatography (IMAC) purification. Each protein was expressed in *Escherichia coli* (*E. coli*) BL21(DE3). The purity and molecular weight of each variant was confirmed with sodium dodecyl sulfate polyacrylamide gel electrophoresis

(SDS PAGE) and matrix-assisted laser desorption/ionization time-of-flight mass spectroscopy (MALDI-TOF-MS) (Figure S1 and S2, Table S2).

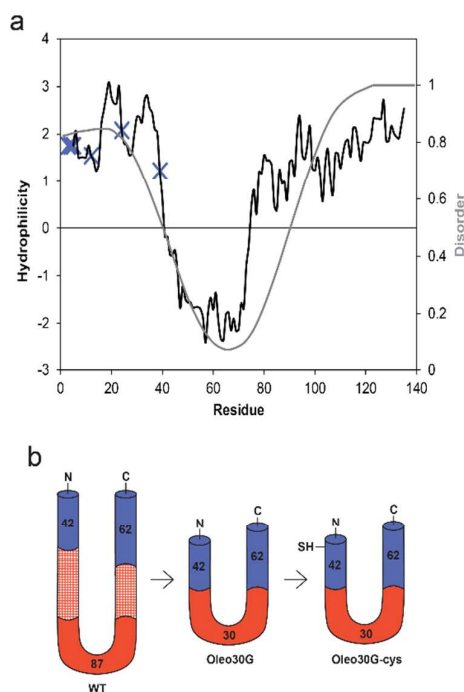


Figure 1. (A) Hydropathy of Oleo30G calculated using the Kyte-Doolittle scale shown in black, left axis. In this plot, positive values indicate hydrophilic residues and negative values indicate hydrophobic residues. Residues that were mutated to a cysteine are indicated with a blue X. Prediction of disorder of Oleo30G made using the PONDR VL3-BA algorithm shown in grey, right axis. Sections with a PONDR score above 0.5 are predicted to be disordered. The N and C terminal segments of Oleo30G are predicted to be both hydrophilic and disordered. (B) Schematics depicting wild type oleosin, Oleo30G, and Oleo30G-cys. The hydrophilic segments are shown in blue and the hydrophobic core is shown in red. Numbers indicate the number of amino acids in each segment. Schematics are simplifications of the protein and do not show the secondary structure. A family of Oleo30G-cys mutants was designed with the single cysteine residue located at various locations in the N-terminal hydrophilic arm.

The secondary structure of the parent molecule, Oleo30G, and of one cysteine mutant, Oleo30G_S2C, was estimated using circular dichroism (CD) (Figure S3). Analysis of the CD spectra show that both Oleo30G and Oleo30G_S2C are largely disordered. Oleo30G is predicted to be 33.9% disordered, and Oleo30G_S2C is predicted to be 34.4% disordered. There is no meaningful difference in the CD spectra between Oleo30G and Oleo30G_S2C, indicating that the incorporation of a cysteine residue does not affect the secondary structure of oleosin.

Assemblies made at low concentrations of Oleo30G and each Oleo30G-cys mutant were investigated using dynamic light scattering (DLS) (Figure S4, Table S3). DLS was conducted with 30 μM protein in Dulbecco's phosphate buffered saline (DPBS) with 1 mM dithiothreitol (DTT). Experiments were conducted at room temperature. For Oleo30G and all Oleo30G-cys mutants, DLS showed a uniform population of assemblies around 20 nm in diameter, which is indicative of spherical micelles.³⁴ The cmcs of Oleo30G and of one cysteine mutant, Oleo30G_S2C, were determined using a pyrene assay

(Figure S5). Oleo30G and Oleo30G_S2C had similar cmcs. Oleo30G had a cmc of 9.36 μM and Oleo30G_S2C had a cmc of 7.30 μM . These results indicate that at low protein concentrations, the addition of a cysteine residue has minimal effect on oleosin self-assembly.

At higher concentrations, both Oleo30G and Oleo30G-cys condensed to form protein droplets. To elucidate the role of the added cysteine in oleosin droplet formation, phase diagrams were developed for Oleo30G and Oleo30G_S2C (Figure 2a-b). Samples were prepared at various protein and salt concentrations. Samples were chilled on ice for 10 minutes before imaging and the presence of droplets was determined visually using brightfield DIC microscopy. For both proteins, droplets form at higher protein concentrations and lower salt concentrations. Considerably lower protein concentrations were needed for droplet formation for Oleo30G_S2C than for Oleo30G. Therefore, the addition of a cysteine residue potentiates liquid-liquid phase separation. For comparison, brightfield differential interference contrast (DIC) images at a protein concentration of 80 μM and at physiological salt concentration (140 mM) are shown for Oleo30G and Oleo30G_S2C (Figure 2c-d). At the same protein and salt concentration, the Oleo30G_S2C droplets are noticeably larger and more numerous than Oleo30G droplets, further suggesting that the addition of a cysteine residue

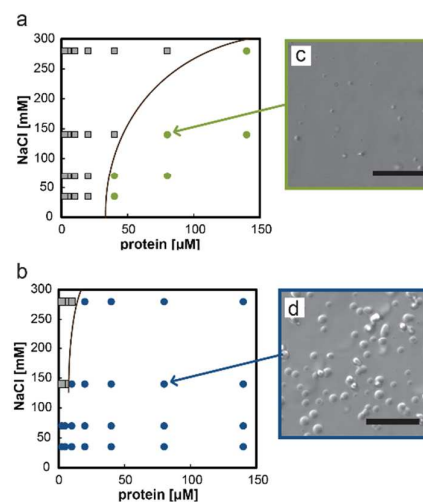


Figure 2. Phase diagrams for Oleo30G (A) and Oleo30G_S2C (B). Compositions at which droplets formed are shown as colored circles and compositions in which droplets did not form are shown as grey squares. As a guide to the eye, an approximate phase boundary is shown. Oleo30G_S2C forms droplets at lower protein concentrations than Oleo30G. Samples were cooled on ice for 10 minutes before imaging on chambered coverglass. The presence of droplets was determined visually. For comparison, Oleo30G and Oleo30G_S2C images are shown in (C) and (D) at the same protein and salt concentration, 80 μM protein and 140 mM salt. At this composition, Oleo30G_S2C droplets are noticeably larger and more numerous than Oleo30G droplets. Scale bars = 20 μm .

potentiates phase separation. We predict that an intermolecular disulfide bond is formed via the cysteine residue on oleosin, creating an additional attractive interaction between oleosin molecules and increasing the propensity to form droplets.

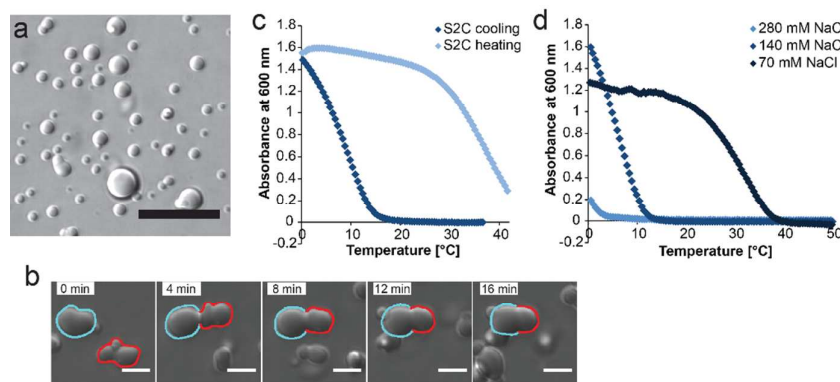


Figure 3. (A) Brightfield DIC microscopy images of Oleo30G_S2C shows spherical droplets. The sample was at a concentration of 80 μM protein in DPBS with 1 mM DTT. The sample was chilled on ice for 10 minutes before transferring to chambered coverglass coated with pluronic F-127. Because the droplets are denser than water, they fell to the bottom of the chamber. Image was taken at the coverglass after droplets settled at the bottom. Scale bar = 20 μm . (B) Time-lapse images of Oleo30G_S2C shows the fusion of two droplets over the course of several minutes. Time starts after droplets settled onto the coverglass. Scale bar = 5 μm . (C) UV-vis spectroscopy traces of Oleo30G_S2C. The sample was at a concentration of 80 μM protein in DPBS with 1 mM DTT. Cooling trace was taken starting at 37 $^{\circ}\text{C}$ and cooling at a rate of 1 $^{\circ}\text{C}$ per minute. An increase in the absorbance indicates the formation of droplets. Heating trace was taken starting at 0 $^{\circ}\text{C}$ and heating at a rate of 1 $^{\circ}\text{C}$ per minute. Return of absorbance to near zero indicates return to a single phase. Measurements were taken in increments of 0.5 $^{\circ}\text{C}$. (D) UV-vis spectroscopy traces of Oleo30G_S2C at various salt concentrations. The sample was at a concentration of 80 μM protein, 1 mM DTT, and salt concentrations of 280 mM, 140 mM, and 70 mM NaCl. Measurements were taken starting at 50 $^{\circ}\text{C}$ and cooling at a rate of 1 $^{\circ}\text{C}$ per minute. Measurements were taken in increments of 0.5 $^{\circ}\text{C}$.

To further characterize the oleosin protein droplets, brightfield DIC imaging was conducted of Oleo30G_S2C at 80 μM protein in DPBS with 1 mM DTT. 1 mM DTT is a common concentration used in protein purifications to prevent irreversible aggregation. The sample was chilled on ice for 10 minutes before imaging. The protein formed micron sized spherical droplets (Figure 3a). The droplets fused upon colliding with one another and contracted towards a spherical shape (Figure 3b), which is typically seen for protein droplets.¹⁶ Droplet fusion occurred on the order of minutes.

The phase transition temperature of Oleo30G_S2C was determined using temperature-dependent ultraviolet-visible spectroscopy (UV-vis) (Figure 3c and S6a). Measurements were taken in DPBS with 1 mM DTT at a protein concentration of 80 μM . An increase in absorbance corresponds to the formation of micron sized droplets. Under these conditions, Oleo30G_S2C has a phase transition temperature of about 12 $^{\circ}\text{C}$. To determine whether the phase transition is thermo-reversible, UV-vis spectroscopy was conducted starting with the protein in the droplet phase and heating to a final temperature of 42 $^{\circ}\text{C}$. The absorbance ultimately decreased to near zero, indicating the droplets had dissolved and the protein had returned to a single phase. There was a significant hysteresis between the cooling and heating curves, with the temperature rising well beyond the cooling phase transition temperature before the droplets dissolved. The dependency of transition temperature on salt concentration was determined using UV-vis spectroscopy (Figure 3d). The transition temperature of Oleo30G_S2C was higher for lower salt concentrations, indicating that lower salt concentrations potentiate phase separation. Dependence of transition temperature on salt is commonly observed for phase separating proteins.¹⁶

Below a critical temperature, the engineered protein Oleo30G_S2C condenses to form micron sized droplets. These droplets are spherical in shape and fuse upon colliding indicating that they are likely liquid droplets. Droplet formation is thermo-reversible; the protein reverts to a single phase upon heating. As is commonly seen in protein droplets, the phase transition temperature is dependent upon the salt concentration.

All the Oleo30G variants considered formed micron sized droplets. DIC images were taken of Oleo30G_S2C, Oleo30G_T3C, Oleo30G_T4C, Oleo30G_T5C, Oleo30G_T12C, Oleo30G_T24C, Oleo30G_S39C, and Oleo30G at 80 μM protein in DPBS with 1 mM DTT (Figure 4). Samples were chilled on ice for 10 minutes before transferring to the chambered

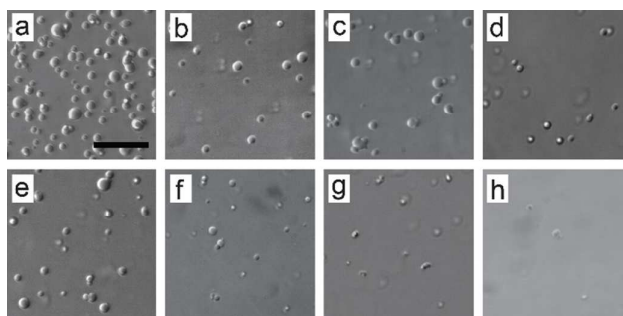


Figure 4. Brightfield DIC microscopy images of (A) Oleo30G_S2C, (B) Oleo30G_T3C, (C) Oleo30G_T4C, (D) Oleo30G_T5C, (E) Oleo30G_T12C, (F) Oleo30G_T24C, (G) Oleo30G_S39C, and (H) Oleo30G. Protein solutions were at a concentration of 80 μM protein in DPBS with 1 mM DTT. Samples were chilled on ice for 10 minutes before transferring to chambered coverglass coated with pluronic F-127. As the droplets are denser than water, they fell to the bottom of the chamber. Images were taken at the coverglass. Scale bar = 20 μm .

coverglass for imaging. Droplets were imaged at room temperature after adding the solution to the chambered coverglass to allowing time for droplets to settle on the coverglass. After imaging, little change was seen to droplet size except for after very long times when droplets would dissolve into the solution. The size of the droplets and number of droplets formed generally decreased for mutants with the cysteine further from the N-terminus of the protein (Table S4).

The transition temperatures for oleosin variants were determined using UV-vis spectroscopy (Figure 5a and S6). For comparison, the temperatures at which the absorbance reached 0.2 were determined (Figure 5b). Oleo30G_S2C had the highest transition temperature. The phase transition temperature fell as the cysteine residue was placed further from the N-terminus of the protein. One hypothesis for this observation is that a cysteine close to the N-terminus of the protein is more accessible and therefore more readily forms disulfide bonds. Likewise, when the cysteine is closer to the hydrophobic core of oleosin it is hindered from forming disulfide bonds. However, further studies would be needed to determine the exact mechanism causing the difference in transition temperature. Nevertheless, the placement of cysteines provides a precise way to tune the phase transition of engineered oleosin protein droplets. For all mutants, the absorbance returned to zero upon heating (Figure S7) indicating that the phase transition is thermo-reversible.

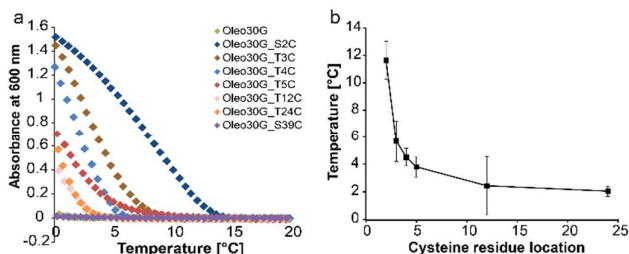


Figure 5. (A) UV-vis spectroscopy traces of Oleo30G and Oleo30G-cys mutants. Protein solutions were at a concentration of 80 μM protein in DPBS with 1 mM DTT. Measurements were taken starting at 37 $^{\circ}\text{C}$ and cooling at a rate of 1 $^{\circ}\text{C}$ per minute. Measurements were taken in increments if 0.5 $^{\circ}\text{C}$. An increase in the absorbance indicates the formation of droplets. For clarity, data is shown only for 20 $^{\circ}\text{C}$ and below. (B) Temperature at which the absorbance measured by UV-vis spectroscopy while cooling at rate of 1 $^{\circ}\text{C}$ per minute reached 0.2 (a.u.) plotted against the position of the added cysteine. Scale bars show the standard deviation from three independent measurements. The transition temperature drops for variants with the cysteine further from the N-terminus of the protein. No values are shown for Oleo30G or Oleo30G_S39C because the absorbance did not reach 0.2.

We predicted that the phase transition temperature could also be tuned by blending Oleo30G and Oleo30G-cys. To test this hypothesis, blends of Oleo30G and Oleo30G_S2C were prepared and the transition temperature of these blends was determined using UV-vis spectroscopy (Figure 6a). Oleo30G_S2C had a transition temperature of about 12 $^{\circ}\text{C}$, Oleo30G had no measurable increase in turbidity, and blends of O30G and O30G_S2C had intermediate transition temperatures, with increasing temperature corresponding to an increase in the amount of Oleo30G_S2C. Therefore, blending Oleo30G and Oleo30G_S2C provides an additional

method to control the phase transition temperature. Brightfield DIC microscopy images of Oleo30G_S2C/Oleo30G blends show micron sized droplets (Figure 6b-f). Droplets of the blends are smaller than droplets of just Oleo30G_S2C. Blends with a higher fraction of Oleo30G_S2C generally formed larger and more numerous droplets than blends with a higher fraction of Oleo30G (Table S5).

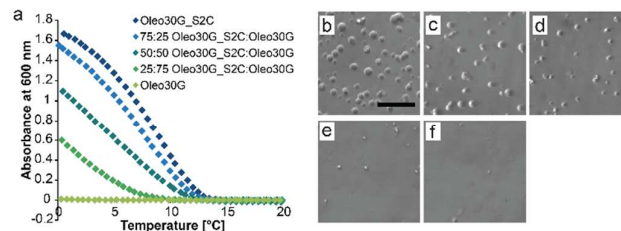


Figure 6. (A) UV-vis spectroscopy traces of Oleo30G_S2C, Oleo30G, and Oleo30G_S2C/Oleo30G blends. Protein solutions were at a concentration of 80 μM protein in DPBS with 1 mM DTT. Blends had a total protein concentration of 80 μM . Blend molar ratios used were 75%/25%, 50%/50%, and 25%/75% Oleo30G_S2C/Oleo30G. Measurements were taken starting at 37 $^{\circ}\text{C}$ and cooling at a rate of 1 $^{\circ}\text{C}$ per minute. Measurements were taken in increments if 0.5 $^{\circ}\text{C}$. An increase in the absorbance indicates the formation of droplets. For clarity, data is shown only for 20 $^{\circ}\text{C}$ and below. Brightfield DIC microscopy images were taken of (B) Oleo30G_S2C, (C) 75%/25% Oleo30G_S2C/Oleo30G, (D) 50%/50% Oleo30G_S2C/Oleo30G, (E) 25%/75% Oleo30G_S2C/Oleo30G, (F) Oleo30G. Solutions were at a total protein concentration of 80 μM in DPBS with 1 mM DTT. Samples were chilled on ice for 10 minutes before transferring to chambered coverglass coated with pluronic F-127. As the droplets are denser than water, they fell to the bottom of the chamber. Images were taken at the coverglass. Scale bar = 20 μm .

Because adding a cysteine residue potentiates phase separation resulting in the formation of droplets, we hypothesized that reducing the disulfide bond formed by the cysteine residues would dissolve the droplets. The reducing agent β -mercaptoethanol (β ME) was added to phase separated protein solutions of Oleo30G_S2C. The protein was

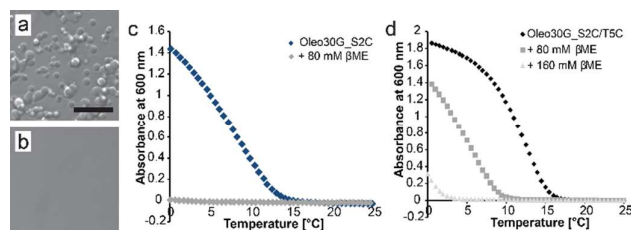


Figure 7. (A) Brightfield DIC microscopy image of Oleo30G_S2C at a concentration of 80 μM protein in DPBS with 1 mM DTT. (B) Brightfield DIC microscopy image of Oleo30G_S2C after the addition of β ME to a final concentration of 80 mM. Samples were chilled on ice for 10 minutes before imaging. Scale bar = 20 μm . (C) UV-vis spectroscopy traces of Oleo30G_S2C. The protein solution was at a concentration of 80 μM protein in DPBS with 1 mM DTT (blue curve). Measurements were taken in increments if 0.5 $^{\circ}\text{C}$ starting at 37 $^{\circ}\text{C}$ and cooling at a rate of 1 $^{\circ}\text{C}$ per minute. Measurements were taken again after addition of β ME to a final concentration of 80 mM (grey curve). For clarity, data is shown only for 25 $^{\circ}\text{C}$ and below. (D) UV-vis spectroscopy traces of Oleo30G_S2C/T5C. Addition of β ME reduced the phase transition temperature of the protein. Unlike the Oleo30G variants containing only a single cysteine, the double cysteine mutant had a measurable increase in turbidity upon cooling after the addition of β ME. Solutions were at a concentration of 80 μM protein in DPBS with 1 mM DTT. Measurements were taken starting at 37 $^{\circ}\text{C}$ and cooling at a rate of 1 $^{\circ}\text{C}$ per minute to a final temperature of 0 $^{\circ}\text{C}$. Measurements were taken in increments if 0.5 $^{\circ}\text{C}$. For clarity, data is shown only for 25 $^{\circ}\text{C}$ and below.

at a concentration of 80 μM and βME was added to a final concentration of 80 mM to be in excess of the protein. After the addition of βME , the turbid, phase separated, protein solution became clear. Brightfield DIC images taken of Oleo30G_S2C droplets before and after addition of βME show that the droplets dissolved to a single phase (Figure 7a-b). UV-vis spectroscopy measurements were taken before and after the addition of βME (Figure 7c). Similar to the cysteine-less parent molecule, reduced Oleo30G_S2C did not show an increase in turbidity at any temperature. All Oleo30G-cys mutants behaved similarly, showing no increase in turbidity after the addition of βME (Figure S8). This finding suggests that the formation of disulfide bonds to form protein dimers is a driving force for liquid-liquid phase separation and that reducing the disulfide bond with βME eliminates this driving force. The addition of reducing agents provides a novel way to control protein droplet dissolution. Oleo30G-cys protein droplets respond to redox conditions and by adding a reducing agent, the droplets can be dissolved.

An Oleo30G variant was made with two cysteine residues, Oleo30G_S2C/T5C. The transition temperature of this two-cysteine mutant was slightly higher than that of Oleo30G_S2C, indicating an increased propensity to form droplets (Figure 7d). βME was also added to the double cysteine mutant Oleo30G_S2C/T5C. Unlike the mutants with only a single cysteine, adding 80 mM βME to the double cysteine mutant was not enough to eliminate the increase in turbidity seen in UV-vis spectroscopy. This result suggests that oleosin variants with two cysteines require more reducing agent to fully reduce the protein.

Discussion

Phase separating proteins have been designed with many properties such as light sensitivity⁷ and protease sensitivity^{5,8}. The effects of factors such as protein charge patterning⁴⁰ and multivalency^{17,18} have also been studied. In this work, we expand the functionality of engineered phase separating proteins by designing a protein with phase transition behavior that is redox sensitive. Previously, polymers have been designed that are sensitive to redox conditions,^{42,43} as well as redox responsive elastin-like polypeptides.⁴⁴ However, although oxidation has been shown to effect protein liquid droplet formation,^{19,20} little work has been done to rationally design redox responsive protein droplets.

We designed redox responsive protein droplets using an engineered recombinant protein. A modified version of the protein oleosin, Oleo30G, was used. Oleo30G consists of a hydrophobic region, flanked by hydrophilic regions. These hydrophilic segments contain both positive and negative charges and are predicted to be disordered, features that are often seen in proteins that undergo liquid-liquid phase separation. At low concentration Oleo30G forms micelles in solution due to the hydrophobic core, however, at sufficiently high concentrations, the protein phase separates to form liquid droplets. We predict that at sufficiently high concentrations the micellar phase condenses, and the

hydrophilic, disordered arms drive phase separation. To increase the intermolecular interactions and enhance phase separation, we added a cysteine residue.

Addition of a cysteine residue to Oleo30G potentiates droplet formation. We hypothesize that this is a result of disulfide bonding between cysteines providing an additional positive interaction between oleosin molecules. Oleosin variants with the cysteine near the hydrophobic core of the molecule have a lower transition temperature than variants with a cysteine close to the N-terminus as demonstrated by UV-vis spectroscopy. The change in transition temperature is likely a steric effect; when the cysteine is buried, disulfide bonds are less likely to form and the driving force for droplet formation is weakened. The phase transition temperature of oleosin droplets can be controlled by varying the location of the cysteine residue or by blending the cysteine-less parent molecule with a cysteine containing variant. In this work, all mutations were done at the N-terminus of the protein, however, it is possible that similar effects may be seen for mutations at the C-terminus. Due to the amenability of oleosin, further work can be done to elicit the effects of other sequence mutations on the phase transition.

We designed protein droplets using an amphiphilic protein to which cysteines have been added, creating droplets that can be dissolved using a reducing agent. The tunable transition temperature and responsiveness to reducing conditions makes Oleo30G-cys droplets attractive for future work designing responsive membrane-less organelles for protocells. These constructs may also have applications in targeted drug delivery. One could envision a system in which a pharmaceutical is encapsulated in the protein droplet and released upon exposure to a reducing environment. Furthermore, the ability to introduce motifs into proteins, such as protease cleavable domains and adhesive motifs, suggests numerous future handles for coordinating the activity of these droplets.

Conclusions

We designed thermo-reversible, liquid protein droplets from recombinant oleosin that are sensitive to redox conditions. To do this, residues in an oleosin variant, Oleo30G, were mutated to introduce a cysteine. These proteins undergo a phase transition below a critical temperature into protein rich droplets surrounded by a protein poor phase. The phase transition temperature can be tuned by varying the location of the cysteine residue in the protein backbone or by blending the cysteine containing variant with the parent molecule. These droplets readily dissolve upon addition of a reducing agent.

Conflicts of interest

There are no conflicts to declare.

Acknowledgements

We are grateful to the NSF Biomaterials program (DMR-1609556) for support. We gratefully acknowledge B. S. Schuster for valuable discussion. We thank A. Tsourkas for use of the spectrophotometer.

References

- S. Alberti, A. A. Hyman, *BioEssays*, 2016, **38**, 959-968.
- C. P. Brangwynne, C. R. Eckmann, D. S. Courson, A. Rybarska, C. Hoeghe, J. Gharakhani, F. Jülicher, A. A. Hyman, *Science*, 2009, **324**, 1729-1732.
- S. F. Banani, H. O. Lee, A. A. Hyman, M. K. Rosen, *Nat. Rev. Mol. Cell Biol.*, 2017, **18**, 285-298.
- V. N. Uversky, *Adv. Colloid Interface Sci.*, 2017, **239**, 97-114.
- M. Amiram, K. M. Luginbuhl, X. Li, M. N. Feinglos, A. Chilkoti, *Proc. Natl. Acad. Sci. U. S. A.*, 2013, **110**, 2792-2797.
- S. M. Sinclair, J. Bhattacharyya, J. R. McDaniel, D. M. Gooden, R. Gopalaswamy, A. Chilkoti, L. A. Setton, *J. Control. Release*, 2013, **171**, 38-47.
- Y. Shin, J. Berry, N. Pannucci, M. P. Haataja, J. E. Toettcher, C. P. Brangwynne, *Cell*, 2017, **168**, 159-171.
- B. S. Schuster, E. H. Reed, R. Parthasarathy, C. N. Jahnke, R. M. Caldwell, J. G. Bermudez, H. Ramage, M. C. Good, D. A. Hammer, *Nat. Comm.*, in press.
- F. G. Quiroz, A. Chilkoti, *Nat. Mater.*, 2015, **14**, 1164-1172.
- S. Holehouse, R. K. Das, J. N. Ahad, M. O. G. Richardson, R. V. Pappu, *Biophys. J.*, 2017, **112**, 16-21.
- W. Pak, M. Kosno, A. S. Holehouse, S. B. Padrick, A. Mittal, R. Ali, A. A. Yunus, D. R. Liu, R. V. Pappu, M. K. Rosen, *Mol. Cell*, 2016, **63**, 72-85.
- P. Brangwynne, P. Tompa, R. V. Pappu, *Nat. Phys.*, 2015, **11**, 899-904.
- W. M. Aumiller Jr., C. D. Keating, *Nat. Chem.*, 2016, **8**, 129-137.
- V. N. Uversky, I. M. Kuznetsova, K. K. Turoverov, B. Zaslavsky, *FEBS Lett.*, 2015, **589**, 15-22.
- M. T. Wei, S. Elbaum-Garfinkle, A. S. Holehouse, C. C. H. Chen, M. Feric, C. B. Arnold, R. D. Priestley, R. V. Pappu, C. P. Brangwynne, *Nat. Chem.*, 2017, **9**, 1118-1125.
- S. Elbaum-Garfinkle, Y. Kim, K. Szczepaniak, C. C. Chen, C. R. Eckmann, S. Myong, C. P. Brangwynne, *Proc. Natl. Acad. Sci. U. S. A.*, 2015, **112**, 7189-7194.
- P. Li, S. Banjade, H. Cheng, S. Kim, B. Chen, L. Guo, M. Llaguno, J. V. Hollingsworth, D. S. King, S. F. Banani, P. S. Russo, Q. Jiang, B. T. Nixon, M. K. Rosen, *Nature*, 2012, **483**, 336-340.
- S. Banjade, M. K. Rosen, *Elife*, 2014, **3**, e04123.
- N. Asherie, J. Pande, A. Lomakin, O. Ogun, S. R. A. Hanson, J. B. Smith, G. B. Benedek, *Biophys. Chem.*, 1998, **75**, 213-227.
- J. Pande, A. Lomakin, B. Fine, O. Ogun, I. Sokolinski, G. B. Benedek, *Proc. Natl. Acad. Sci. U. S. A.*, 1995, **92**, 1067-1071.
- J. L. Frandsen, H. Ghandehari, *Chem. Soc. Rev.*, 2012, **41**, 2696-2706.
- Hammer, N. P. Kamat, *FEBS Lett.*, 2012, **586**, 2882-2890.
- X. Huang, A. J. Patil, M. Li, S. Mann, *J. Am. Chem. Soc.*, 2014, **136**, 9225-9234.
- G. I. Frandsen, J. Mundy, J. T. C. Tzen, *Physiol. Plant.*, 2001, **112**, 301-307.
- S. C. Bhatla, V. Kaushik, M. K. Yadav, *Biotechnol. Adv.*, 2010, **28**, 293-300.
- L. G. Alexander, R. B. Sessions, A. R. Clarke, A. T. Tatham, P. R. Shewry, J. A. Napier, *Planta*, 2002, **214**, 546-551.
- K. Hsieh, A. H. C. Huang, *Plant Physiol.*, 2004, **136**, 3427-3434.
- M. C. M. Chen, C. Chyan, T. T. T. Lee, S. Huang, J. T. C. Tzen, *J. Agric. Food Chem.*, 2004, **52**, 3982-3987.
- M. Rayner, *Curr. Opin. Food Sci.*, 2015, **3**, 94-109.
- M. T. Chang, T. R. Tsai, C. Y. Lee, Y. S. Wei, Y. J. Chen, C. R. Chen, J. T. C. Tzen, *J. Agric. Food Chem.*, 2013, **61**, 9666-9671.
- J. Chiang, C. J. Chen, L. J. Lin, C. H. Chang, Y. P. Chao, *J. Agric. Food Chem.*, 2010, **58**, 11695-11702.
- L. Parmenter, J. G. Boothe, G. J. H. van Rooijen, E. C. Yeung, M. M. Moloney, *Plant Mol. Biol.*, 1995, **29**, 1167-1180.
- K. Sharma, M. K. Sharma, *Biotechnol. Adv.*, 2009, **27**, 811-832.
- K. B. Vargo, N. Sood, T. D. Moeller, P. A. Heiney, D. A. Hammer, *Langmuir*, 2014, **30**, 11292-11300.
- K. B. Vargo, R. Parthasarathy, D. A. Hammer, *Proc. Natl. Acad. Sci. U. S. A.*, 2012, **109**, 11657-11662.
- Gao, K. B. Vargo, D. A. Hammer, *Macromol. Biosci.*, 2016, **16**, 1398-1406.
- K. B. Vargo, A. A. Zaki, R. Warden-Rothman, A. Tsourkas, D. A. Hammer, *Small*, 2015, **11**, 1409-1413.
- N. Sreerama, R. W. Woody, *Anal. Biochem.*, 2000, **287**, 252-260.
- B. Xue, R. L. Dunbrack, R. W. Williams, A. K. Dunker, V. N. Uversky, *Biochim. Biophys. Acta - Proteins Proteomics*, 2010, **1804**, 996-1010.
- J. Kyte, R. F. Doolittle, *J. Mol. Biol.*, 1982, **157**, 105-132.
- K. P. Sherry, R. K. Das, R. V. Pappu, D. Barrick, *Proc. Natl. Acad. Sci. U. S. A.*, 2017, **114**, E9243-E9252.
- S. Cerritelli, D. Velluto, J. A. Hubbell, *Biomacromolecules*, 2007, **8**, 1966-1972.
- M. Huo, J. Yuan, L. Tao, Y. Wei, *Polym. Chem.*, 2014, **5**, 1519-1528.
- Xu, D. Asai, A. Chilkoti, S. L. Craig, *Biomacromolecules*, 2012, **13**, 2315-2321.

Inserting cysteine into oleosin yields redox sensitive protein droplets; the phase transition temperature depends on the location of the cysteine.

